The Φ-Operator: A Rotation Operator For Flow Analysis and Visualization *

Guoning Chen†, Lei Zhang†, David Thompson‡, Adrian Sescu‡, and Robert S. Laramee§

Department of Computer Science
University of Houston
Houston, TX, 77204, USA
http://www.cs.uh.edu

Technical Report Number UH-CS-14-02

July 14, 2014

Keywords: Vector fields, integral curves, signed curvature, streaklines.

Abstract

A prevalent strategy in vector field data analysis is to extract and classify the integral curves derived from flow data. With the exception of topology-based methods, many of these classifications depend on the choice of algorithm thresholds. However, topology-based methods have yet to be fully developed for time-varying vector field analysis. In this paper, we introduce a novel descriptor, called the $\Phi-$operator for flow data analysis that is based on the *signed curvature* of an integral curve. With this descriptor, the vector-valued data analysis is reduced to a scalar field analysis problem. We present the definition and computation of the Φ field and show how to utilize it to achieve a flow domain partitioning based on the behaviors of the integral curves seeded at different spatial locations. A unified framework for the computation of the Φ field and its gradient field, $|\nabla\Phi|$, is introduced. This framework is easy to implement and can be applied to the characterization of streamlines, pathlines, and streaklines based on their different geometric attributes. A new flow feature, referred to as *cycloid boundary curves*, corresponding to the ridges of the $|\nabla\Phi|$ field is revealed that classifies the flow domain into regions with different rotational behavior. We apply this framework to the analysis and visualization of a number of synthetic and simulation flow data sets. Finally, we provide a detailed comparison of this new structure with a number of well-known flow features, including vector field topology, vortex regions, FTLE ridges, and singularity paths. Our comparison shows that collectively the Φ and $|\nabla\Phi|$ fields encode more flow information than previous individual feature descriptors alone.

*This work was supported by the National Science Foundation, IIS-1352722.
†Guoning Chen and Lei Zhang are with University of Houston
‡ David Thompson and Adrian Sescu are with Mississippi State University
§Robert S. Laramee is with the Swansea University, UK.

The Φ-Operator: A Rotation Operator For Flow Analysis and Visualization *

Guoning Chen†, Lei Zhang†, David Thompson‡, Adrian Sescu‡, and Robert S. Laramee§

Abstract

A prevalent strategy in vector field data analysis is to extract and classify the integral curves derived from flow data. With the exception of topology-based methods, many of these classifications depend on the choice of algorithm thresholds. However, topology-based methods have yet to be fully developed for time-varying vector field analysis. In this paper, we introduce a novel descriptor, called the $\Phi-$operator for flow data analysis that is based on the *signed curvature* of an integral curve. With this descriptor, the vector-valued data analysis is reduced to a scalar field analysis problem. We present the definition and computation of the Φ field and show how to utilize it to achieve a flow domain partitioning based on the behaviors of the integral curves seeded at different spatial locations. A unified framework for the computation of the Φ field and its gradient field, $|\nabla\Phi|$, is introduced. This framework is easy to implement and can be applied to the characterization of streamlines, pathlines, and streaklines based on their different geometric attributes. A new flow feature, referred to as *cycloid boundary curves*, corresponding to the ridges of the $|\nabla\Phi|$ field is revealed that classifies the flow domain into regions with different rotational behavior. We apply this framework to the analysis and visualization of a number of synthetic and simulation flow data sets. Finally, we provide a detailed comparison of this new structure with a number of well-known flow features, including vector field topology, vortex regions, FTLE ridges, and singularity paths. Our comparison shows that collectively the Φ and $|\nabla\Phi|$ fields encode more flow information than previous individual feature descriptors alone.

Index Terms

Vector fields, integral curves, signed curvature, streaklines.

I. Introduction

Vector field analysis is a ubiquitous approach that is employed to study a wide range of dynamical systems. Applications involving vector fields include automobile and aircraft engineering, climate study, combustion dynamics, earthquake engineering, and medicine, among others. With the continuous increase in size and complexity of the resulting flow data sets, there is a strong demand to develop an effective abstract representation that does not increase the complexity of data interpretation and user interaction.

One popular solution to meet this need is to compute the *topology* of the flow data. The computation of topology in some sense serves the purpose of dimensionality reduction of the original data, i.e., it condenses the original data into its skeletal representation; thus, a lower-dimensional descriptor with sparse visual primitives can be employed to convey the structural information of the flow data effectively. Because of these useful properties, vector field topology has been successfully applied to the analysis of steady flow [1], [2], [3], [4].

However, there are a number of fundamental limitations of flow analysis based on vector field topology. Most importantly, the conventional vector field topology 1) does not apply to time-dependent vector fields and 2) only encodes hyperbolic features in the flow (i.e., vortices are not included). A large body of recent work has been dedicated to extending the notion of topology to enhance the understanding of time-dependent vector fields. Among them, the most successful and popular solution is the *Finite Time Lyapunov Exponent (FTLE)* approach that characterizes the separation behavior of the flow particles based on their pathlines [5]. The Lyapunov exponent measures the rate of the separation of nearby flow particles over time. The computation of the FTLE values at spatial samples can be used to derive a scalar field. The ridges of this scalar field, defined as the *Lagrangian Coherent Structures (LCS)*, indicate the regions of the domain with relatively high separation. They correspond to the regions where the flow particles are unlikely to cross, i.e., curves or surfaces with negligible flux. Due to its

*This work was supported by the National Science Foundation, IIS-1352722.
†Guoning Chen and Lei Zhang are with University of Houston
‡ David Thompson and Adrian Sescu are with Mississippi State University
§Robert S. Laramee is with the Swansea University, UK.

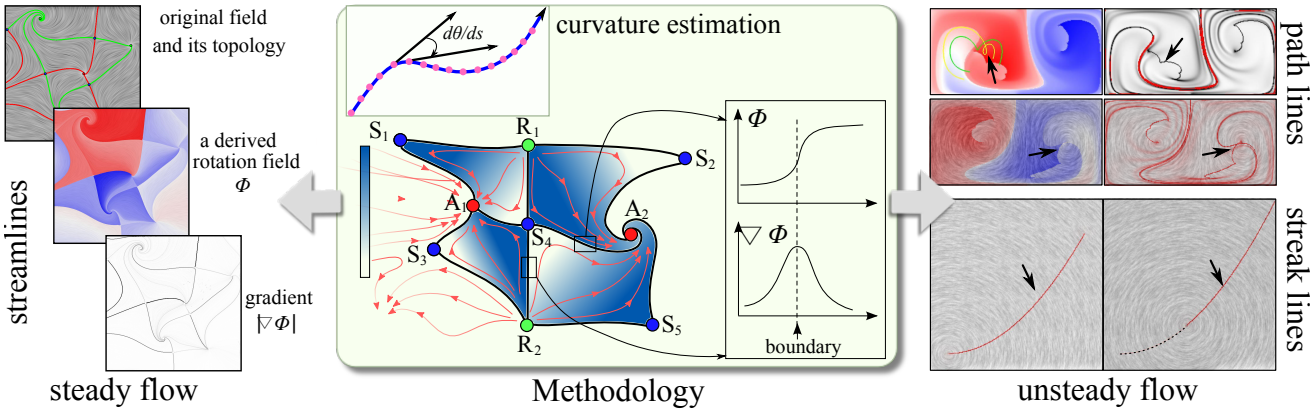

Fig. 1. Illustration of our methodology and its applications to both steady and unsteady flow based on streamlines, pathlines, and streaklines, respectively. The left images show the application to the steady flows. Arrows on the upper right images indicate the new features, namely cycloid boundary curves. The lower right images show that the proposed framework can be used to identify the singularity paths.

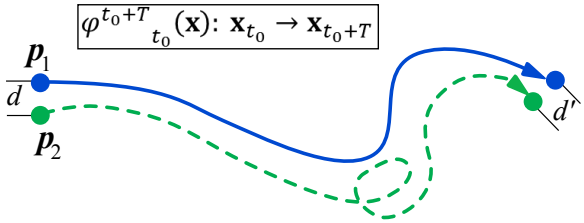

Fig. 2. An example in which the FTLE approach may not capture the different behaviors of nearby particles.

ability to characterize flow separation behavior, which is similar to the vector field topology, the FTLE approach has received extensive attention recently. However, like vector field topology, FTLE does not consider rotation in the flow. In addition, the computation of FTLE may not extract important flow behavior as it only measures the Euclidean distances between the starting and ending points of nearby particles. Figure 2 provides an example. The distance, d', between the end positions of two particles, $\mathbf{p}_1$ and $\mathbf{p}_2$, does not change noticeably compared to their distance, d, at seeding positions. Therefore, the associated FTLE value is relatively small. However, the pathlines themselves show rather different behaviors. Specifically, $\mathbf{p}_2$ has an additional 2π rotation. This difference is not highlighted by FTLE. Finally, the definition of FTLE does not apply to *streaklines*, an important type of feature curves that have been studied extensively in experimental fluid dynamics [6]. This motivates the presented work.

In this paper, we generalize the previously introduced *winding angle* concept [7] and extend it to the definition and computation of a scalar field derived from the flow data, which we refer to as a Φ *field*, in a similar fashion to the FTLE field computation. The winding angle is defined as the accumulated rotation of an integral curve. It has been used as a binary operator to identify vortices in the flow. That is, the streamlines with winding angles larger than some user-specified threshold may indicate the presence of vortices in the flow. In this work, we point out that the winding angle is intrinsically related to the total curvature of a curve. We observe that, in addition to highlighting the flow rotation behavior, this total curvature information can be used to identify other flow structures, such as flow separation. Furthermore, we apply this curvature estimation to both pathlines and streaklines under a unified framework, and show how it can be used to extract and visualize a new and previously unidentified flow structure.

The contributions of this work can be summarized as follows.

- We introduce a $\Phi-$operator based on the curvature computation. Using this $\Phi-$operator, a derived scalar field, i.e., the Φ field, is computed. We show that in regions with *similar flow behavior* (e.g., similar rotation behavior) the variance of this Φ field is smooth, while larger changes occur across the boundaries of regions with dissimilar rotation behavior. This is well-captured by the gradient of the Φ field, denoted by $\nabla\Phi$. A new skeletal structure that is comprised of the ridges of $|\nabla\Phi|$ is derived that corresponds to the boundaries of the regions with different rotational behavior.
- We present a unified computation framework for the Φ and $|\nabla\Phi|$ fields based on different attributes along

different types of integral curves, including streamlines, pathlines, and streaklines. As both Φ and $|\nabla\Phi|$ are scalar fields, we apply simple visualization techniques, such as color plots with well-designed transfer functions, to convey the flow structure information encoded in these fields.

- We provide detailed comparison of the Φ and $|\nabla\Phi|$ fields with a number of well-known flow features, including the flow separation, boundary features, and vortices. In particular, we show that the structure revealed by the Φ and $|\nabla\Phi|$ fields encodes not only the flow separation structure but also other information, such as vortices and boundary switch points in steady flows, as well as new structure that is previously unidentified in unsteady flows.
- We observe an important drawback of accumulating attributes along pathlines for the unsteady flow analysis, and promote analysis and visualization based instead on streaklines. This view is supported by our experiments in feature tracking.

Despite its many useful properties, there are still some limitations of the proposed method, e.g., it does not apply to timelines. Therefore, rather than claiming it is a better measure for flow analysis, we consider the proposed analysis and visualization framework a valuable complement to existing flow analysis techniques.

II. Related Work

There is a large body of literature on the analysis and visualization of flow data. Interested readers are encouraged to refer to recent surveys [8], [9], [3], [10], [11] that provide systematic classifications of various analysis and visualization techniques. In this section, we focus on the most relevant work that attempts to classify different integral curves based on a selection of similarity metrics.

A. Vector Field Topology

Vector field topology provides a streamline classification strategy based on the origin and destination of the individual streamlines. And more importantly, this classification is *parameter-free* for steady vector fields.

Since its introduction to the visualization community [2], vector field topology has received extensive attention. A large body of work has been introduced to identify different topological features, including fixed points [12], [13], [4] and periodic orbits [1], [14], [15]. Recently, Chen et al.[16] studied the instability of trajectory-based vector field topology and, for the first time, proposed Morse decomposition for vector field topology computation, which leads to more a reliable interpretation of the resulting topological representation of the vector field. In order to minimize the dependency on the numerical integration, Reininghaus et al. [17] applied the combinatorial theory of Forman [18] to study the topology of 2D flows. Recently, Reich and Scheuermann studied streamline separation using time-discrete Markov chains [19].

The demonstrated success of vector field topology in the analysis of steady vector fields has inspired efforts to extend it to the analysis of unsteady vector fields. The most successful strategies are based on the Lyapunov exponent. Specifically, *Lagrangian Coherent structures (LCS)* were introduced to identify separation structure for pathlines under time-dependent settings. The computation of LCSs was first introduced by Haller [5] by computing the *Finite Time Lyapunov Exponent (FTLE)* of the flow. Using FTLE fields computed using forward and backward time integrations, two scalar fields are derived whose values are high in areas of diverging and converging flow, respectively. LCSs are then defined as the ridge-lines/-surfaces of the two FTLE fields with negligible flux [20], [21]. Since its introduction, FTLE has been compared with the separatrices in the steady cases [22], [23], and its computation performance has been improved substantially [24]. Compared to the strategies that employ the FTLE, our visualizations generally provide additional flow structure information. Further, our method can be applied to streaklines, while the FTLE approach only applies to pathlines. This is significant because, as we will demonstrate, pathline-based approaches do not encode as much information about the temporal variation in the flow as our streakline-based approach. Finally, our framework uses a simpler pipeline than the FTLE-based strategies.

Recently, Sadlo and Weiskopf introduced a streakline-based topology based on the concept of generalized streaklines [25]. It successfully characterizes the saddle type of hyperbolic features. This was extended to study the 3D unsteady flow topology [26]. Similar to the FTLE approach, this generalized topological notion does not encode the rotational dynamics of the flow. We demonstrate how analyzing the rotation behavior of streaklines can provide such information.

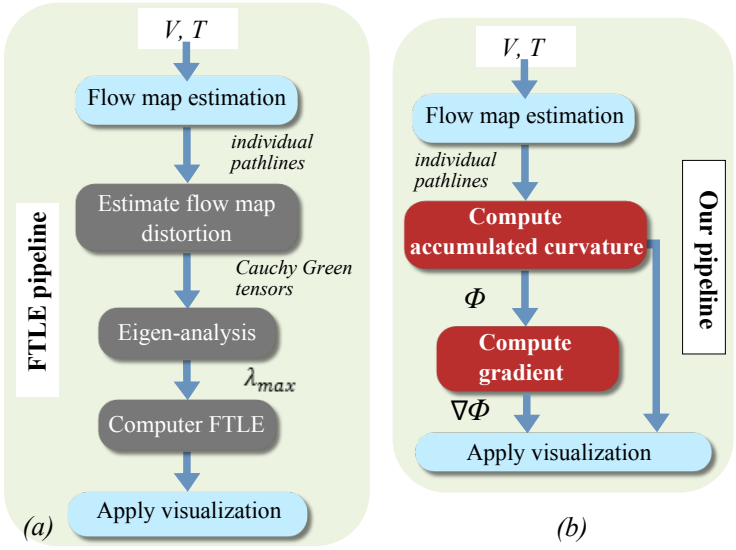

Fig. 3. (a) The FTLE computation pipeline, (b) our pipeline.

B. Other Classification Approaches

a) Streamline and pathline attributes: Sadarjoen and Post introduced the winding angle concept for streamlines and utilized it to classify the streamlines within vortical regions [7]. In contrast, our work does not make a binary decision for feature detection. Salzbrunn and Scheuermann introduced *streamline predicates*, which classify streamlines by interrogating them as they past through certain user-specified features, e.g., vortices [27]. Later, this approach was extended to the classification of pathlines [28]. At the same time, Shi et al. presented a data exploration system to study the different characteristics of pathlines based on their various attributes, including winding angles [29]. Recently, a statistics-based method was proposed to help select the proper set of pathline attributes to improve the interactive flow analysis [30]. Our work differs from the pathline predicate and pathline attribute in that it utilizes the attributes of the individual pathlines to construct a smooth scalar field to classify the spatial locations where pathlines are seeded. This enables us to study the flow structure as well as to classify the integral curves. There are other techniques for classifying streamlines that are constrained to the flow separation and vortex structures. The recently introduced streamline bundling technique [31] is such an example. A survey [11] provides a more detailed review on this topic. More recently, McLoughlin et al. introduced the idea of a streamline signature based on a set of curve-based attributes including curvature and torsion [32]. This streamline signature is used to compute the similarity between streamlines, and help domain experts place and filter streamlines for the creation of an informative and uncluttered visualization of 3D flow.

b) Information theory framework: A more recent direction for scientific data visualization is to consider it as a visual communication channel in which the input is the raw data and the output is the result of a visualization. Information theory can be applied to evaluate the effectiveness of the visualization by measuring how much information present in the original data is conveyed through the visual communication channel [33]. Based on this premise, Xu et al. [34] introduced an information-theoretic framework for flow visualization so that more streamlines are placed in regions with large information entropy, indicating large variance of certain flow quantities, e.g., vector orientation. This large variance is typically associated with important flow dynamics, e.g., fixed points and vortices. Lu et al. [35] extended this framework to take into account the detailed curvature information of the individual streamlines for effectively classifying the streamlines with similar curvature distributions. This work is the most relevant to the presented method. The important difference is that, rather than computing curvature, which relies on higher-order derivative computation we use the rotation of the tangent vectors along the integral curves that are provided directly by the vector field with no additional computation. In addition, the segmentation strategy built on top of the proposed rotation operator can be used to assist both user controlled classification of the integral curves and the automatic segmentation of the flow domain similar to the partitioning obtained based on flow topology.

III. Framework Overview

Figure 3(a) describes the pipeline of the computation of an FTLE field from a given vector field. The computation of FTLE estimates the flow map distortion of an unsteady vector field by computing the spatial distance between particles that are initially seeded next to each other [5]. According to Section IV-A, the set of all trajectories of a time-dependent vector field provides the flow map $\varphi_{t_0}^{t}(\mathbf{x})$ with the position at time t on the trajectory starting at time t_0 from $\mathbf{x}_0$. By computing the flow map gradient and left-multiplying it with its transpose, the *Cauchy deformation tensor*, ∇, can be derived which is proportional to the rate-of-strain tensor. In the limit $t \to t_0$, the FTLE is the maximum principal rate-of-strain, that is, the maximum eigenvalue of ∇. For a more formal and detailed discussion, the reader is encouraged to refer to Haller's seminal work [5].

Our unified analysis and visualization framework also starts with a flow map estimation. Next, we estimate the curvature along individual integral curves, and assign these values to their corresponding seeding positions. This provides the rotation field, Φ. Then, we calculate the gradient of the Φ field, i.e., $\nabla\Phi$. Finally, we visualize the Φ field and the magnitude of its gradient, denoted by $|\nabla\Phi|$, using color plots with a selection of transfer functions. Figure 3(b) illustrates our pipeline. Compared to the FTLE computation, our pipeline is easier to implement and can be integrated into an existing FTLE computation pipeline. In addition, it can be adapted to streaklines and utilize other curve properties to study the similar characteristics of feature curves. We will describe these extensions in a later section. In the following, we will concentrate on the theory and computation of the Φ field and its gradient.

IV. The Rotation Field Φ and Its Gradient

In this section, we start with a brief review of the basic vector field concepts. Then, we will generalize the previously introduced winding angle computation and discuss its relationship with the local curvature along an integral curve. Next, we describe how to accumulate local curvature for the construction of the Φ field.

A. Vector Field Background

Consider a d-manifold $\mathbb{M} \subset \mathbb{R}^d$ ($d = 2,3$ in our cases. A velocity field is a vector field that can be expressed as an ordinary different equation $\dot{\mathbf{x}} = V(\mathbf{x},t)$ or a map $\varphi : \mathbb{R} \times \mathbb{M} \to \mathbb{R}^d$, satisfying $\varphi_{t_0}^{t_0}(\mathbf{x}) = \mathbf{x_0}$ and $\varphi_{t_0}^{t+s}(\mathbf{x}) = \varphi_{s}^{t+s}(\varphi_{t_0}^{s}(\mathbf{x})) = \varphi_{t}^{t+s}(\varphi_{t_0}^{t}(\mathbf{x}))$. This flow map describes the spatial correlation of points through *trajectories* (or flow paths) starting at time t_i: $\varphi_{t_i}^{t}(\mathbf{x})$. A linearization of the local variation of the map $\varphi_{t_0}^{t}(\mathbf{x})$ around a point $\mathbf{x_0}$ is obtained by considering its spatial gradient $J_{\mathbf{x}}(t_0,\mathbf{x_0}) = \nabla_{\mathbf{x_0}}\varphi_{t_0}^{t}(\mathbf{x_0})$ at $\mathbf{x_0}$. In the static case, this linearization can be expressed as $LV(\mathbf{x_0}) = V(\mathbf{x_0}) + J_{\mathbf{x}}(\mathbf{x_0})V$. Intuitively, the first term provides the *translation* of the flow, while the second term encodes the flow *kinematics* (or deformation) [36], [37].

There are a number of curves that describe different aspects of the translational property in vector fields.

- A *streamline* is a solution to the initial value problem of the ODE system confined to a given time t_c: $\mathbf{x}_{t_c}(t) = \mathbf{p}_0 + \int_0^t V(\mathbf{x}(\eta);t_c)d\eta$.
- *Pathlines* are the paths of the massless particles released in the flow domain at a given time t_0: $\mathbf{x}(t) = \mathbf{p}_0 + \int_{t_0}^{t} V(\mathbf{x}(\eta);t_0+\eta)d\eta$.
- A *streakline*, $\tilde{s}(t) = \bigcup_{t_0}^{t}\mathbf{x}_{t_i}(t)$ where $\mathbf{x}_{t_i}(t)$ is the current position of particle p_i that was released from position p_0 at time t_i.
- A *timeline*, $\tilde{\tau}(t) = \bigcup_i \mathbf{x}_i(t)$ where $\mathbf{x}_i(t)$ is the current position of particle p_i released at time t_0.

In steady vector fields, streamlines, pathlines, and streaklines are identical. Among these curves, only streamlines and pathlines are integral curves of the original flow field by definition. They represent particle advection under steady and unsteady conditions, respectively. Many techniques have been proposed to classify streamlines or pathlines based on their different behaviors. In particular, for the steady case, the vector field topology is defined as the connectivity of flow recurrent features including *fixed points* and *periodic orbits* [1]. Fixed points correspond to the places where vector values vanish, or $\varphi(t,\mathbf{x}) = \mathbf{x}$ for all $t \in \mathbf{R}$. A periodic orbit corresponds to a flow path that is closed, or mathematically, a trajectory that passes through a point $\mathbf{x}$ such that $\varphi(t,\mathbf{x}) = \mathbf{x}$ for a non-zero t.

B. The Curvature of An Integral Curve

Consider an integral curve, $\mathscr{C}$ of a vector field V and its arc-length parameterization $\mathscr{C}(s)$ ($s \in [0,1]$). The curvature at any given point $\mathscr{C}(s)$ is defined as $\kappa(s) = T'(s)\cdot\mathbf{n}(s)$, where $T'(s) = \frac{dT(s)}{ds}$ and $\mathbf{n}(s)$ is the normal of $\mathscr{C}$

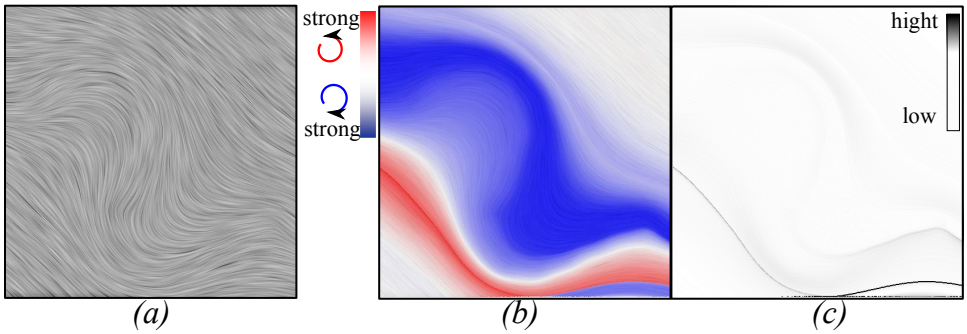

Fig. 4. An example of Φ field (b) and its gradient magnitude field $|\nabla\Phi|$ (c). (a) shows the LIC of the flow.

at s. The accumulated (or net) curvature of $\mathscr{C}$ from a starting point to a parameter value $L \in [0,1]$ is then defined as

$$\Phi_{\mathscr{C}}(L) = \int_0^L \kappa(s) ds \tag{1}$$

If $L = 1$, Eq.(1) computes the total curvature of $\mathscr{C}$. In particular, $\Phi_{\mathscr{C}}(L) \geq 2\pi$, if $\mathscr{C}$ is closed.

At the same time, $\kappa(s) = \pm|T'(s)|$ and $|T'(s_0)| \approx |\frac{T(s_0+ds)-T(s_0)}{ds}| = |\frac{\tilde{V}(\mathscr{C}(s_0+ds))-\tilde{V}(\mathscr{C}(s_0))}{ds}| \approx |\frac{d\theta}{ds}|$, where $\tilde{V}(\mathscr{C}(s_0))$ is the normalized velocity vector defined at $\mathscr{C}(s_0)$, and $d\theta$ denotes the angle change between $\tilde{V}(\mathscr{C}(s_0+ds))$ and $\tilde{V}(\mathscr{C}(s_0))$. This equation holds because an integral curve in the flow field, such as a streamline or a pathline, is tangent to the vector field everywhere based on its definition. In 2D vector fields, $d\theta > 0$ if $\tilde{V}(\mathscr{C}(s_0+ds))$ is rotated counter-clockwise with respect to $\tilde{V}(\mathscr{C}(s_0))$, while $d\theta < 0$ if the rotation is clockwise. Eq.(1) can be *approximated* by the accumulation of this sign angle rotation:

$$\Phi_{\mathscr{C}}(L) = \int_0^L \frac{d\theta}{ds} ds \tag{2}$$

It is also worth mentioning that the curvature at point $\mathscr{C}(s_0)$ is defined as $\frac{V\times\mathbf{a}}{|V|^3}$ [32], where $\mathbf{a} = (\Delta V)V(\mathscr{C}(s_0))$ is the local acceleration and can be decomposed as $\mathbf{a} = a_T\mathbf{T} + a_n\mathbf{n}$ where a_T is the tangent component of the acceleration and a_n is the normal component. We then have

$$\frac{V\times\mathbf{a}}{|V|^3} = \frac{V\times(a_T\mathbf{T}+a_n\mathbf{n})}{|V|^3} = \frac{a_T(V\times\mathbf{T})+a_n(V\times\mathbf{n})}{|V|^3} = \frac{a_n(V\times\mathbf{n})}{|V|^3}$$

where we use $V\times\mathbf{T} = 0$ since V is collinear with T. $\frac{V}{|V|}\times\mathbf{n}$ returns a vector perpendicular to the plane defined by V and $\mathbf{n}$. Therefore, we have $a_n = \kappa|V|^2$. This is expected because the normal acceleration is a representation of the change in the direction of the velocity vector, which resembles the angle rotation defined in Eq.(2).

In practice, the accumulation of Eq.(2) can be approximated by the computation of the *winding angle* along the integral curve $\mathscr{C}$ that consists of N integration points P_i and $(N-1)$ line segments (P_i, P_{i+1}) [7]:

$$\Phi_{\mathscr{C}}|_{L=1} \approx \alpha_{\mathscr{C}} = \sum_{i=1}^{N-1} d\theta_i \tag{3}$$

where $d\theta_i = \angle(P_{i-1}, P_i, P_{i+1}) \in (-\pi, \pi]$ represents the angle between two consecutive line segments.

To avoid confusion, we will refer to this accumulation as the total rotation, Φ, along $\mathscr{C}$ in the rest of the paper.

C. The Φ Field and Its Gradient $\nabla\Phi$

Given any point $\mathbf{x} \in M$, there is a scalar function $f(L) = \Phi(\mathscr{C}_{\mathbf{x}}(L))$ that measures the total rotation of the integral curve starting from $\mathbf{x}$. We refer to the derived scalar field as the Φ field. The gradient of Φ is defined as $\nabla\Phi = (\frac{\partial\Phi}{\partial x}, \frac{\partial\Phi}{\partial y})$. It is well-known that $\nabla\Phi$ points to the direction where Φ increases the fastest, and its magnitude $|\nabla\Phi|$ indicates the rate of variation of Φ in this direction. In particular, larger $|\nabla\Phi|$ values denote locations where the Φ value changes more rapidly. This typically indicates the transition between regions with different rotational behavior (Figure 1, middle). In other words, large changes in Φ highlight flow structural information determined by the rotational behavior of integral curves.

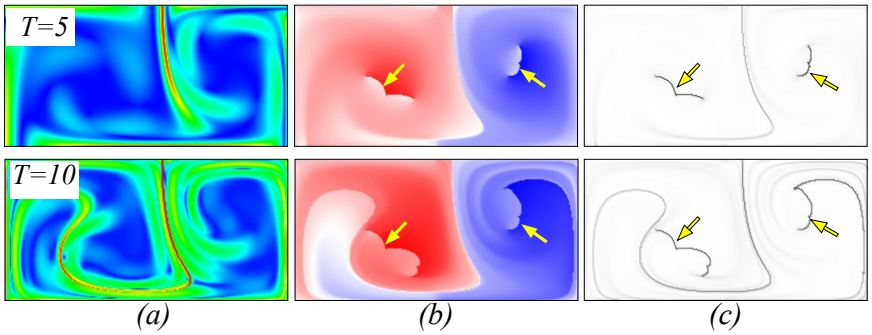

Fig. 5. The FTLE (a), Φ (b), and $|\nabla\Phi|$ (c) fields of a double gyre flow with $T = 5$ (top) and $T = 10$ (bottom). With larger values of T, more details of the flow structure can be revealed. The yellow arrows highlight new cusp-like edges that will be discussed in Section V-B.

To visualize a Φ field, we utilize a blue-white-red color coding scheme. The blue-white-red color is particularly useful to highlight the two opposite rotational behaviors, i.e., blue for regions with smaller Φ values, and red for regions with larger Φ values (Figure 4(b)). To visualize $|\nabla\Phi|$, we map the values that are smaller than the median to white, and the values that are above the median to gray colors from white (smaller) to black (larger). This high contrast visualization enables us to view the flow structure easily (Figure 4(c)).

1) Computation of Φ and $|\nabla\Phi|$ Field: The computation of the Φ fields depends on the types of feature curves that we use to examine their rotational behavior. For pathlines of an unsteady flow, we employ a *regular sampling* strategy, e.g., $M \times N$, to place seeds in the domain. From each seed $\mathbf{x}$, a pathline is integrated over time T using a $4^{th}-$order Runge-Kutta integrator. A linear interpolation scheme is applied in both space and time during integration. The accumulated curvature (based on Eq. 2) is computed and assigned to point $\mathbf{x}$. To handle the boundary of the domain, we let the particle advect with a constant velocity at the boundary for the remaining time. After obtaining a Φfield, $\nabla\Phi$ can be estimated at each sample position by computing the gradient of Φ.

a) Streamlines: To handle streamlines for the analysis of steady flow, we need to slightly modify the above computation. In particular, from each seeding position, we trace a streamline in both the forward and backward directions. For the forward tracing, we simply sum up $d\theta$ over the integration, while for backward tracing, we sum $-d\theta$. In addition to the reaching the maximum integration time (or maximum number of integration steps in steady cases), there are other termination conditions, including 1) reaching a fixed point, 2) hitting the flow domain boundary, or 3) forming a closed loop. Note that these additional termination conditions are not applied to the unsteady flow analysis.

b) Φ fields with varying integration time T: As described above, the integration time T is an important user-specified parameter that may affect the analysis and visualization results. This is similar to its effect on FTLE computations. Generally, the larger T is, the more detailed structure that may be revealed, while the smaller T is, the coarser the flow structure. This matches what has been observed for FTLE computations. Figure 5 shows the FTLE (a), Φ (b), and $|\nabla\Phi|$ (c) fields of a double gyre flow [25] with $T = 5$ and $T = 10$, respectively. The new structure, which we call a cycloid boundary curve, is highlighted. In the steady case, instead of using an integration time, we use the number of integration steps to control the length of the streamlines. Similarly, the larger the number of integration steps the more detailed the structure that is extracted. For all the steady flow results, we use $4N$ as the maximum number of integration steps, where N is the resolution of the samples in the X or Y direction, e.g. 512.

V. Results and Discussion

In this section, we discuss the application of the proposed rotation operator to the analysis of a number of synthetic and simulated 2D vector fields. We will show how the proposed Φ and $|\nabla\Phi|$ fields compare to a number of important well-known flow features in the literature. In the following, we first concentrate on the application to steady vector fields, then we provide our results and insight for unsteady flow.

A. Application to Steady Vector Fields

We have applied this technique to a number of synthetic data sets (Figures 4, 7, 8, 9) and the 2D slices of cross sections of a diesel engine simulation (Figure 6) [1]. All of these results demonstrate the utility of the Φ field and

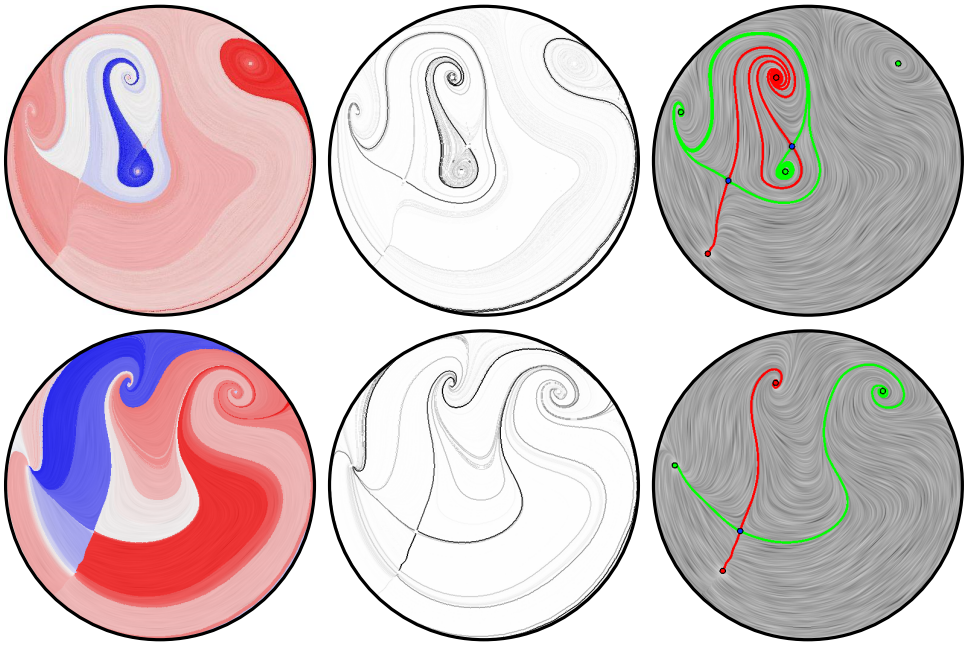

(a) *(b)* *(c)*

Fig. 6. The analysis and visualization from the cross sections of a diesel engine simulation [38]. (a) Φ fields; (b) $|\nabla\Phi|$ field; (c) topology.

its gradient for steady flow visualization. The computation cost of this implementation is determined largely by the sampling resolution and the integration scheme employed. For most of the steady flow results shown in the paper with 512×512 resolution, a 4^{th}-order Runge Kutta integrator was used. The computation time was between 1 and 1.5 minutes on a PC with Intel(R) Xeon(R) 1.6GHz quad-core processor and 8GB RAM without parallelization.

1) Comparison With Feature-Based Flow Visualization Techniques: From these results, we demonstrate the correlation of the flow structure highlighted by Φ and $|\nabla\Phi|$ fields with a number of well-known features in steady flow.

a) Comparison to topological segmentation: An important observation is that the Φ field has similar values inside a topologically homogeneous region, or *basin*, in which all streamlines start from identical origin (e.g., a source) and end at identical destiny (e.g., a sink). Figure 7(b) shows the plots of the Φ (top) and $|\nabla\Phi|$ (bottom) values along two line segments through which a number of streamlines traverse (Figure 7(a)). Due to the uniqueness of streamlines in a steady vector field, all the points along the same streamline have the same Φ value. Therefore, the Φ values obtained along this line segment correspond to the Φ values of the streamlines intersecting with these line segments. From the top plot, we see that the variation of the Φ values along the line segment within a homogeneous region (green) is gradually decreasing (i.e., the gradient field is almost flat (bottom plot)). This reflects the expected smooth transition of the geometric characteristics of neighboring streamlines within a homogeneous region. In contrast, the Φ field encounters a steeper gradient across the separation structure (or boundary) of two homogeneous regions (e.g., the magenta line segment and its corresponding plots in Figure 7). The gradient of the Φ field there exhibits a spike, i.e., a large local maximum (see the bottom plot of Figure 7(b)). This is because the flow paths on the two sides of a separation structure typically have *opposite* rotational behaviors in a 2D continuous vector field without degenerate features (e.g., singularity lines) (Figure 7(c)).

This observation enables us to develop a visualization based on Φ and $|\nabla\Phi|$ fields to highlight flow separation structure. However, similar to FTLE results, we cannot conclude that the ridges of the $|\nabla\Phi|$ field correspond to the topology of the vector field. Instead, the selected ridges based on a given threshold values reveal the separation structures of varying strengths. For the steady results shown here, we do not impose any explicit threshold but rather design a simple transfer function to highlight the ridges (see Section IV-C). Therefore, certain important separation structures that may correspond to the separatrices of the topology may be missed in the resulting visualization due to their smaller $|\nabla\Phi|$ values. In addition, when this transfer function is applied to the unsteady flow (Section V-B), certain aliasing artifact can be observed in the visualization of the ridges of the $|\nabla\Phi|$ fields, i.e., some pixels

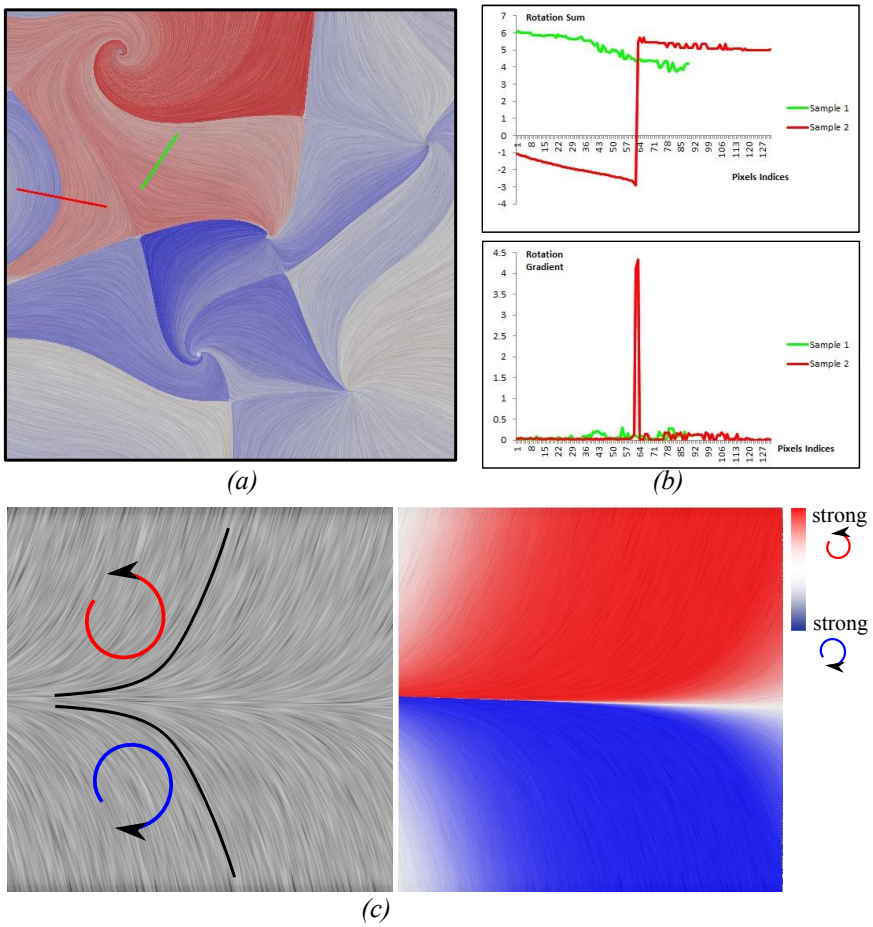

Fig. 7. Φ field in a homogeneous region and cross the separation boundary of two neighboring homogeneous regions. The two colored line segments in (a) indicate the sampled lines for the two groups of streamlines. (b) shows the plots of the Φ and $|\nabla\Phi|$ values along the two line segments, respectively. (c) illustrates that the flow separation typically indicates the opposite rotations of the particle trajectories starting at different sides of a separation structure, which helps explain what is observed in (a) and (b).

on the ridges may or may not be lit (see the accompanying videos). In the future, more robust ridge extraction techniques can be employed to locate these weaker features in order to capture a more complete description of the flow structure and address the aliasing artifact.

b) Additional boundary features: The Φ and $|\nabla\Phi|$ fields also highlight the locations of boundary switch points that indicate the transition of inflow and outflow with respect to the flow domain (rather than the image) boundary. More particularly, there exists a streamline at each boundary switch point that is tangent to the boundary, i.e., the flow inner tangency (places where trajectories are tangent to the boundaries without leaving the domain). This tangent streamline partitions the domain into an outer segment and an interior segment, respectively, where the streamlines in the outer segment are closer to, likely starting from and ending at the boundary, than those located in the interior segment. These two groups of streamlines have rather different Φ values. This enables the $|\nabla\Phi|$ field to highlight the boundary between these regions. Figure 8 provides two examples in which the boundary switch points are highlighted automatically (as indicated by the arrows). In addition, the separation lines starting at the boundary saddle points that separate the inflow streamlines and outflow streamlines are visible. However, as these boundary features are sensitive to the configuration of the domain boundaries, they should be used as complementary information to the flow structure.

2) Comparison with vortex region: The definition and computation of the Φ field relies on the estimation of the curvature of the streamlines. It is natural to compare our analysis and visualization results based on Φ to *vortices*. Although there is no a unified definition of a vortex, the general consensus is a vortex is comprised of highly rotating (or convoluting) streamlines. That said, these streamlines will have large absolute winding angles (or accumulated curvature) [7]. However, a proper threshold to measure the region boundary is difficult to define. To test its ability of locating the vortex regions, we apply our analysis framework to a synthetic 2D flow that consists of a number

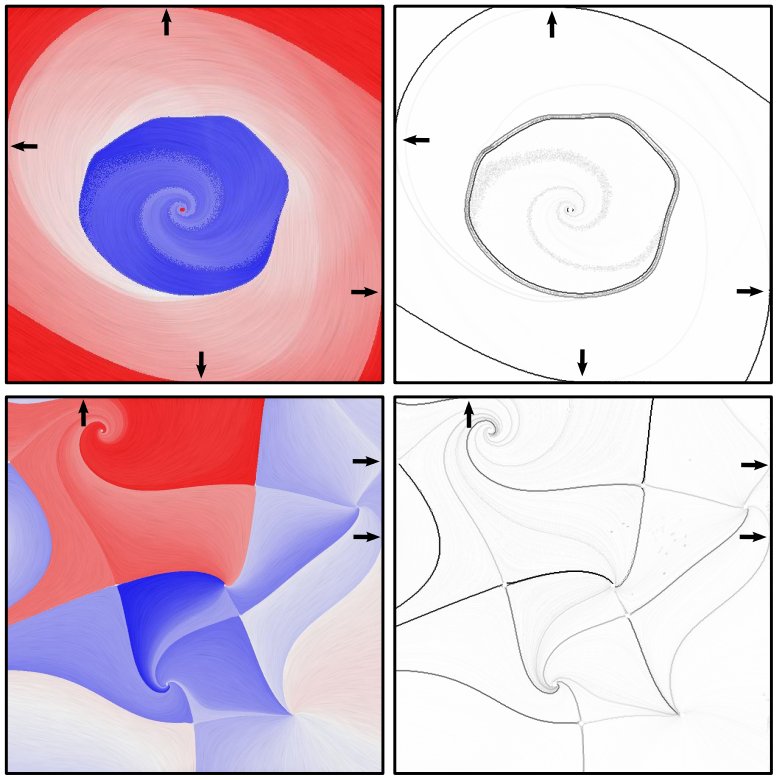

Fig. 8. The Φ and $|\nabla\Phi|$ fields highlight additional features not included in traditional topology, such as the inner tangent flow with respect to the boundary, i.e., boundary switch points, pointed out by the arrows.

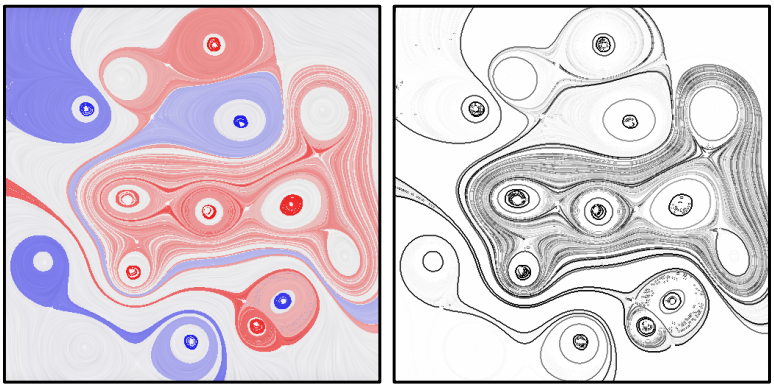

Fig. 9. The Φ and $|\nabla\Phi|$ fields highlight vortex regions.

of centers (a special type of vortex) (Figure 9). Interestingly, it seems that the $|\nabla\Phi|$ field forms silhouettes at the boundaries of certain vortices. At the same time, we also notice a large gray portion in the middle right of the image. This is caused by numerical inaccuracy. Ideally, streamlines around a center should be closed. However, due to integration error, the streamlines may not be closed and circle around until the specified maximum number of integration steps is reached. This is a well-known numerical issue encountered in practice [16]. In this example, an adaptive $4^{th}-$order Runge-Kutta integrator is employed.

These comparisons to various flow features remind us of another important and popular flow descriptor, the well-known parallel vectors (or PV) operator [39], which can be used to identify the locations of separation and vortical flows. However, the PV operator is a local estimator, and is subject to the accuracy of the higher-order derivative approximation. Therefore, the results based on the PV operator can be noisy and rely on the choice of a non-intuitive threshold. In contrast, the proposed $\Phi-$operator is a global metric (i.e., measured along feature curves) and does not require the computation of a higher-order derivative. Therefore, the derived results are typically smoother and contain less noise. However, the definition and computation of the Φ field depends on the chosen numerical integration scheme. The quality of the Φ field largely depends on the accuracy of the integrator, an issue

that we leave for future work.

B. Application to Unsteady Vector Fields

We have applied the Φ and $|\nabla\Phi|$ field computation and visualization framework to a number of unsteady flow data sets, including a double gyre flow [5], [25] (Figure 11) and a flow behind a cylinder [40] (Figure 12), to demonstrate its utility. Similar to FTLE, we start with the study of the behavior of pathlines that reveals the dynamics of the flow.

a) Comparison with FTLE: To compare our results with those obtained using the FTLE approach, we implemented a simple FTLE computation framework where a uniform sampling strategy is employed. Figure 11 shows the forward FTLE (a), Φ (b), and $|\nabla\Phi|$ (c) fields at three sampled time steps for the double gyre flow. We set $T = 10$ for this example. The costs for computing the FTLE fields and Φ fields are similar at about 33 and 34 seconds, respectively, for a 256 sampling resolution for the double gyre flow without parallelization on a PC with Intel Core i7-3537U CPU and 8GB RAM.

To compare the FTLE ridges with the ridges of $|\nabla\Phi|$ field, we first identify the positions whose FTLE values are larger than a user-specified threshold, e.g., $0.65 f_{max}$ for this example (f_{max} is the maximum FTLE value). We then highlight these locations in red on the visualization of the $|\nabla\Phi|$ field (Figure 11(d)). From this visual comparison, we see that the $|\nabla\Phi|$ field captures very similar behavior to the FTLE field. In addition, there exists additional structure encoded in the $|\nabla\Phi|$ field that is not captured in the FTLE field. In particular, this additional structure attaches to the center of the four vortices, shown by the underlying LIC texture. In order to understand what flow dynamics induce this feature, we sampled a number of particles at two different sides of this structure and examine the behaviors of the obtained pathlines. As shown in Figure 10, the pathlines seeded at different sides of the structure have different rotational behavior. One can observe a similar behavior in the cycloid motion. Thus, we refer to this cusp-like edges as *cycloid boundaries*. Particularly, the pathlines on one side of the structure have an additional turn (shown as a self-intersecting loop), whereas they do not on the other side. In addition, the pathlines seeded exactly on the cycloid boundaries exhibit the same cycloid behavior of a rolling disk along the four yellow line segments that highlight the dynamic paths of the four vortices. This helical behavior of pathlines in space and time domain may indicate the existence of vortices over time. This information is not captured by the FTLE field. This example further demonstrates that the ridges of the $|\nabla\Phi|$ field encode not only flow separation structures but also the boundaries of regions in which the pathlines seeded have different rotational behavior. This information can be used to help domain experts place particles for an interactive study of the flow behaviors, similar to the strategy employed in a recent work on streamline seeding [32].

b) Backward integration: Our operator can be applied to both forward and backward time integration. Figure 12 (a2) shows the results for a flow past a cylinder [40]. The top three rows show the forward results with $T = 3$, while the middle three rows show the backward results with $T = -3$. (a3) shows the visualization obtained by combining the extracted forward (red) and backward (blue) ridges of the $|\nabla\Phi|$ field. It took about 90 seconds to compute one frame for the results shown in Figure 12(a). Please refer to the supplementary video for the complete animations of the unsteady flow results.

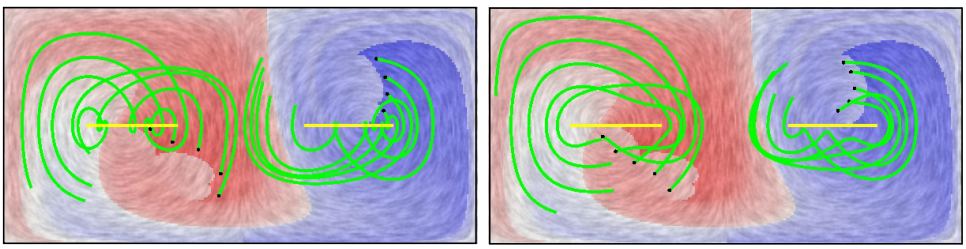

(a) *(b)*

Fig. 10. The pathlines sampled at two sides of the additional cusp-like feature near the vortex centers of the double gyre flow. There is cycloid-like rotation along the pathlines seeded on the right hand side (a), while the pathlines seeded on the other side do not possess this behavior (b). Therefore, we call this new feature a cycloid boundary. The four yellow line segments are *manually* added to highlight the paths of the four moving vortices.

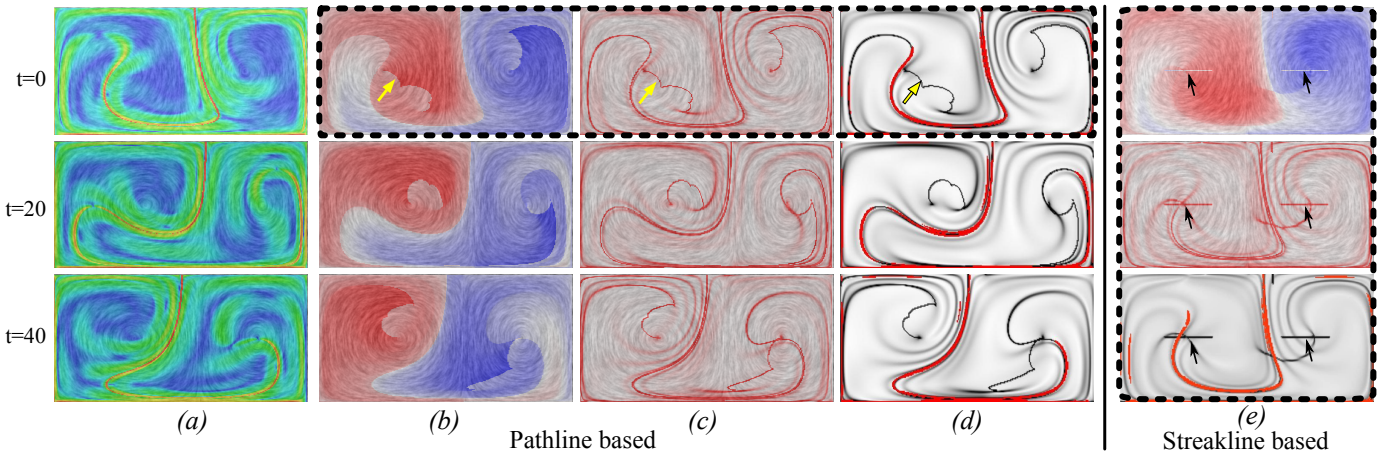

Fig. 11. The analysis results of a double gyre flow [25]. (a-d) at the right of the figure shows the forward FTLE, Φ fields, $|\nabla\Phi|$ fields, and the comparison of LCS and $|\nabla\Phi|$ ridges at a number of sampled time steps, respectively. For FTLE, a rainbow color coding is used where red indicates larger FTLE values and blue smaller. A blue-white-red color map is used for the Φ field with red for larger Φ values and blue for smaller values. A white-red color map is used to visualize $|\nabla\Phi|$ field with red for larger values and lighter red and white for smaller values. For the comparison of LCS and $|\nabla\Phi|$ ridges (d), the extracted FTLE ridge points are highlighted in red on top of the $|\nabla\Phi|$ visualization that utilizes a gray scale color map. (e) shows the results based on streaklines at $t = 0$. Compared to the pathline-based results (see the two dash rectangles), the streakline-based analysis captures the singularity paths of the two vortices over time as highlighted by the black arrows, while the pathline-based analysis only highlights the cycloid boundaries (indicated by the yellow arrows).

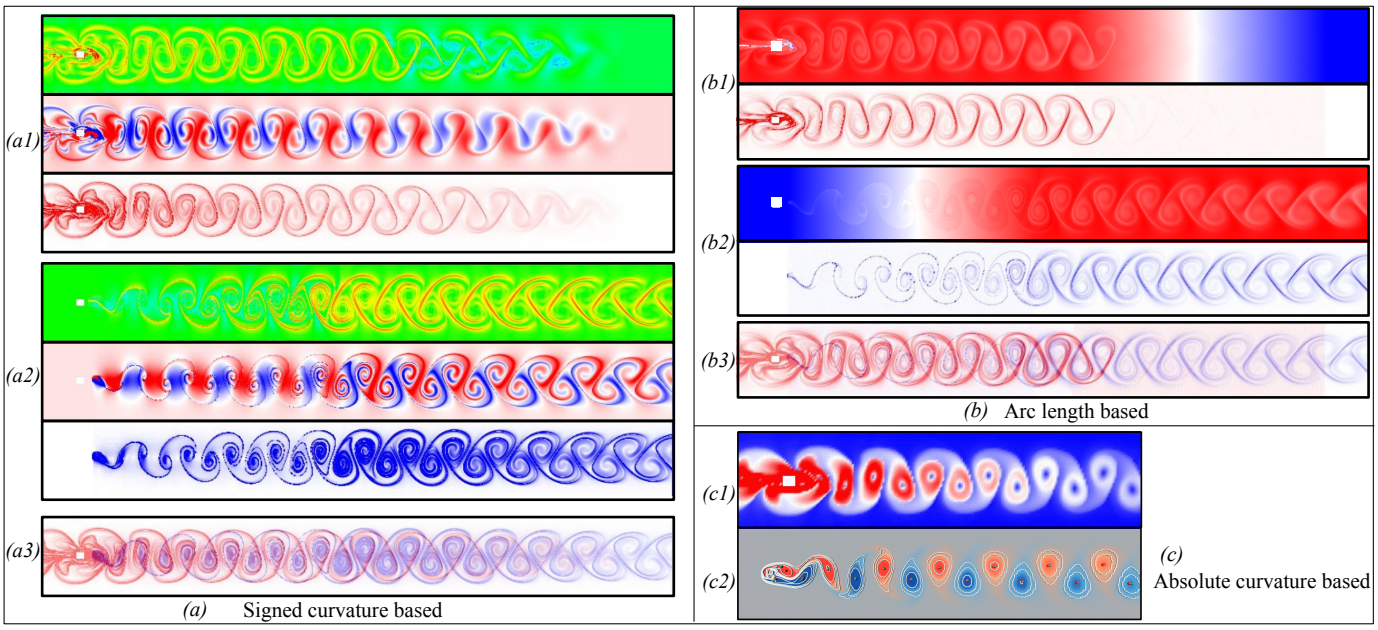

Fig. 12. The analysis results of the flow past a cylinder simulation. (a) shows the results based on the computation of Φ of the pathlines: (a1) the forward tracing results with FTLE in the top row followed by the Φ and $|\nabla\Phi|$ fields (a2) the backward tracing results, and (a3) the combination of the forward (red) and backward (blue) ridges of $|\nabla\Phi|$ fields. (b) shows the results based on the arc-lengths of the pathlines: (b1) the forward tracing results with the length field at the top followed by its gradient, (b2) the backward tracing results, and (b3) the combination of the forward and backward ridges of the gradient of the two length fields. (c) shows the comparison of the Φ field computed using absolute curvature (c1) with the vorticity iso-lines from[41] (c2).

VI. Extension and Discussion

In this section, we describe an extension of our approach to other geometric attributes of the integral curve. Then, we discuss the limitations of the presented method.

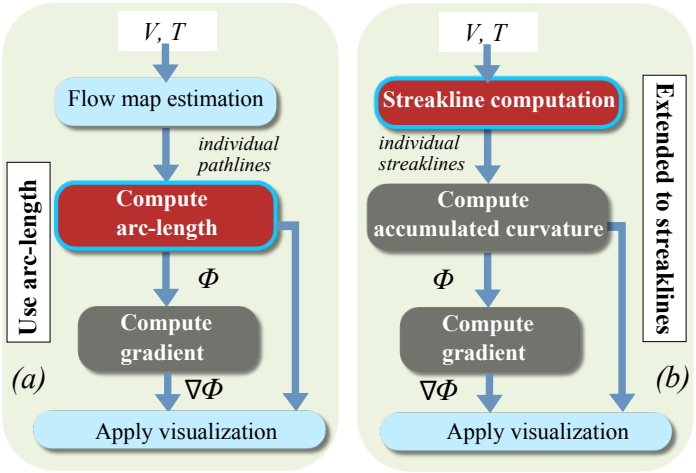

Fig. 13. (a) measures the arc-lengths of the derived individual curves and assign them to their corresponding seeding positions, (b) extends to the analysis of streaklines.

A. Extension to Other Attributes

In addition to utilizing the curvature of the integral curves to classify their behaviors, other attributes that reveal different geometric and physical aspects of the integral curves can be employed, such as those used in [32], [29]. In the following, we show two extensions. First, we modify the curvature computation that computes Φ along the integral curves with *sign*. Instead, we accumulate the *absolute* angle change, i.e., $\Phi(\mathscr{C})(L) = \int_0^L \frac{|d\theta|}{ds} ds$. This enables us to address the possible cancellation of the accumulation of signed rotation (Section VI-B). However, the information about the orientation of the rotation is lost. Figure 12 (c) compares the modified Φ field with the vorticity iso-line extraction [41] of the flow behind a cylinder. From this comparison, we see the new Φ field silhouettes the regions of the vortices similar to the vorticity iso-lines. However, the difference is we use *pathlines* instead of streamlines to compute the Φ field.

Another intrinsic attribute of an integral curve is its arc-length. We modify our general pipeline (Figure 13(a)) to measure the lengths of the individual integral curves. Figure 12 (b) provides an example on the flow behind a cylinder. Similar to the different rotational behavior of the integral curves on different sides of a separation structure, these curves have different lengths. In particular, the length of the integral curve along the separation structure should be shorter than its nearby integral curves based on the theory of FTLEs. This observation allows us to use a similar framework to highlight the separation structure, i.e., the lengths of the integral curves have larger change across a separation structure.

Note that the arc-length has no sign, which is similar to the absolute accumulated curvature. Therefore, it cannot distinguish the different (rotation) behaviors of the integral curves on opposite sides of a separation structure.

B. Limitations

c) Signed Rotation Cancellation: It is possible that negative rotation cancels out the positive in some symmetric flow where the integral curves exhibit *sine function* like fluctuation (Figure 14 (a)). This may not be desired as the rotation information is lost (i.e., zero net curvature). However, in vortex identification, this cancellation may help distinguish the spiral streamlines from those exhibiting certain rotational behavior but not forming vortices. Figure 14(b) shows an airfoil flow. The vortex regions are clearly highlighted (as can be seen in the zoom in view of Figure 14(b)), while the other non-vortex areas are reasonably suppressed even though the flow there exhibits non-zero rotation. Note that the separation flow near the head of the airfoil is not highlighted. This is because the rotation of the streamlines seeded at different sides but near the separation have almost zero Φ values. To address this, a metric that examines and compares the local curvature behavior rather than the accumulated behavior using certain binning strategy along the integral curves as proposed in the work [35], [32] can be employed. We will investigate this in our future work.

d) Challenges of accumulating attributes along pathlines: It is worth reiterating that our method captures the boundaries between spatial regions from which released particles exhibit varying rotational behavior. However, this approach and, for that matter, any approach that assigns values accumulated along a pathline to a field location,

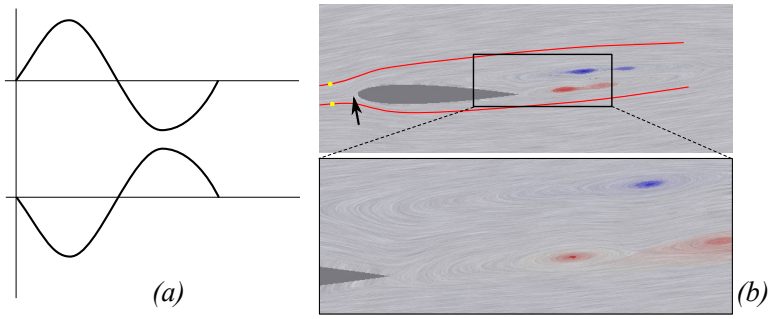

Fig. 14. (a) an illustration of the fluctuated streamlines where their accumulated rotation is zero. (b) an airfoil flow (bottom image shows the zoom in view). The two red lines are sampled streamlines passing through the two yellow seeds, respectively. Their respective Φ values are similar. Therefore, the separation flow near the head of the airfoil (highlighted by the arrow) is not highlighted by Φ.

may produce features that do not necessarily exhibit spatio-temporal correlation with the particle release points. For example, in Figure 11(b-d), the cusp-like features do not correlate with regions in the flow that exhibit strong rotation. This is because the accumulation process may incorporate the dynamical event (e.g., strong rotation) that occurs at a different location and at a later time to the seeding location as long as they are correlated by the same pathline. In contrast, the FTLE field, which does not employ an accumulated value but instead represents the rate of divergence (convergence) of particles released from a region, does accurately reflect the spatial location of the divergence. Nonetheless, our method does provide a classification for pathlines based on the similarity of their rotational behavior.

Motivated by the challenges of accumulating attributes along pathlines, in the following, we describe the extension of our framework to streaklines along which the accumulation of attributes may provide more useful and interesting information about the flow.

VII. Streakline-based Φ

One unique characteristic that our analysis framework can offer when compared to the FTLE method is that the Φ field computation can be applied to any smooth integral curves derived from the flow. Figure 13 (b) illustrates the modified pipeline that incorporates streaklines by replacing the flow map estimation step with the streakline computation. In our current implementation, we use the same spatial sampling employed to compute the pathlines for the streaklines. Figure 11(e) shows the Φ and $|\nabla\Phi|$ results for the double gyre flow. To reduce the memory overload, we limited the number of particles released for each streakline to 200. This may affect the smoothness of streaklines depending on the time window T for the computation. The current way we handle boundaries is to terminate the computation of a streakline once any of its particles hit a boundary.

From the results shown in Figure 11(e), we notice four edge segments in the visualization (highlighted with arrows), while the other flow structure intersects and rotates around them. Based on the information shown in the background LIC, these four line segments correspond to the dynamic trajectories of the centers of the four vortices. This causes us to conjecture that the Φ and $|\nabla\Phi|$ fields computed based on streaklines can highlight the trajectory of certain moving singular features (i.e., with zero vector values at some given time steps). To verify this conjecture, we performed a number of additional experiments on synthetic unsteady vector fields. Specifically, we placed a number of representative 2D singularities (such as center, sink/source, and saddle) and translated them along a prescribed path over time. Figure 15 illustrates the results. Interestingly, the highlighted ridge structures of the $|\nabla\Phi|$ fields indeed correspond to the paths of singularities in the simple cases without bifurcations (i.e., Figure 15 $(a-d)$), despite that they cannot distinguish the difference between those features. To understand why this occurs, we sampled a number of streaklines on and just off the highlighted ridges and studied their geometric properties. Figure 16 corresponds to the scenario of a moving center. Note that a rapid direction change is exhibited for each streakline sampled *on* the ridge of the $|\nabla\Phi|$ field (Figure 16(b)). This cusp-like sharp turn becomes an additional 2π rotation when the seeding position is moved to below the ridge (Figure 16(c)).

e) Discussion: In general, the Φ field computed based on streaklines encodes more temporal information than the Φ field based on pathlines. This is because a streakline consists of the end points (at a given time t) of a set of pathlets generated from different flow maps $\varphi_{t_i}^{t}(\mathbf{x}_0)$ starting at fixed location $\mathbf{x}_0$ but varying t_i. Thus, the streakline-based Φ encodes temporal variation in the flow map through variation in t_i. For example, the motion of

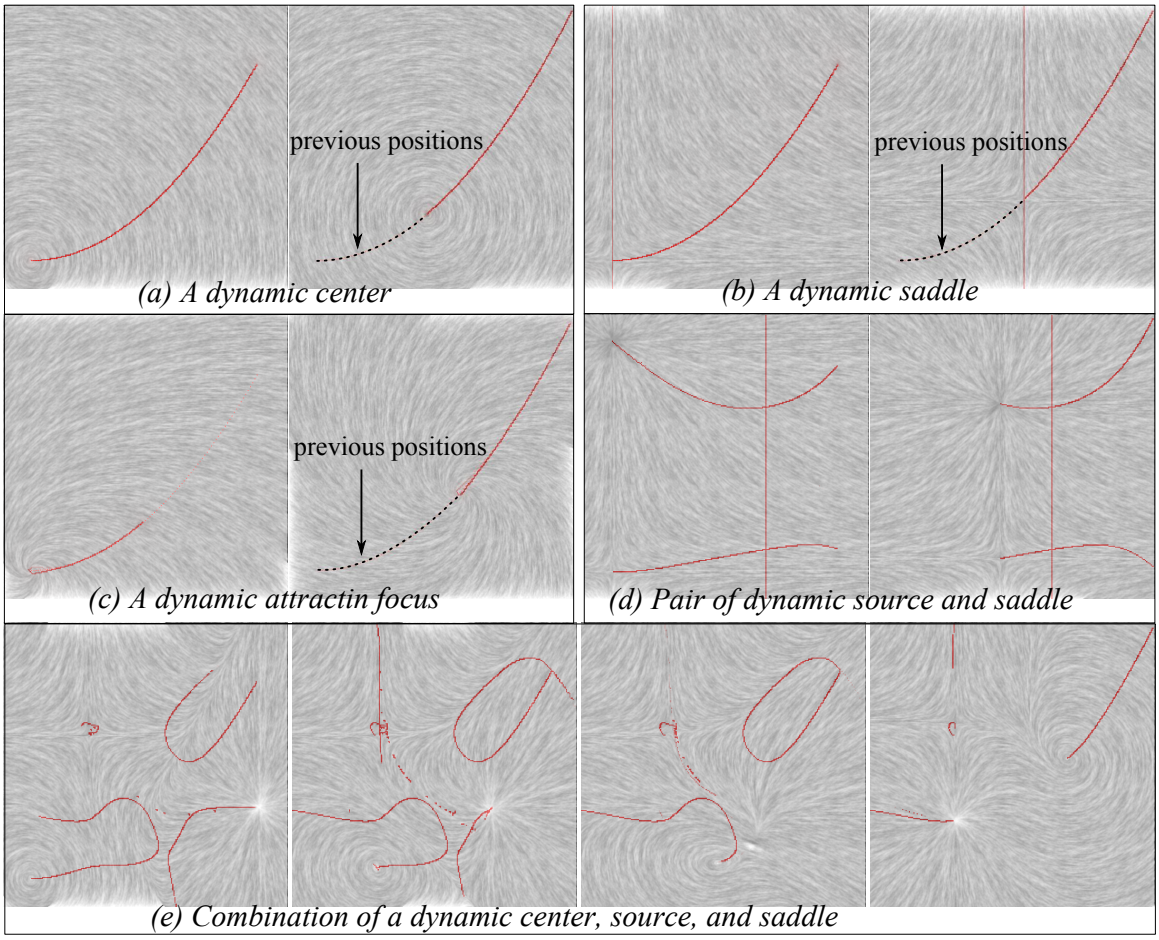

Fig. 15. The $|\nabla\Phi|$ fields based on streaklines for a number of synthetic unsteady flows. Please refer to the accompanying videos for the complete animations.

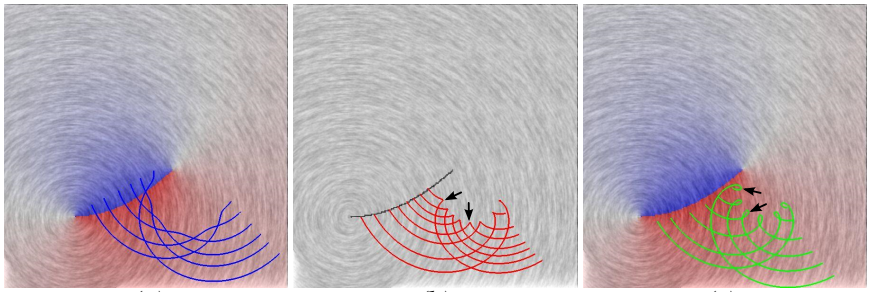

Fig. 16. (a) shows the streaklines (blue) sampled above the ridge of the $|\nabla\Phi|$ field that highlights the path of a moving center. (b) shows the streaklines (red) sampled on the ridge, while (c) shows the streaklines (green) sampled below the ridge. Note that there exhibits a (cusp-like) sharp turn for each streakline sampled on the ridge, much similar to the cycloid motion we observe in Figure 10. The streaklines sampled below the ridge as in (c) have additional 2π rotation compared to those sampled above the ridges (a).

the singularities cannot be revealed by pathlines (Figure 11) because this motion reflects a temporal variation at $\mathbf{x}_0$ that cannot be captured by the pathline computed using the flow map initiated at a *single time*. In the meantime, this motion is reflected by the streakline-based approach (Figure 11(e)) because the subsequent particles released at later times will capture this temporal variation.

Figure 15(e) also shows a complex scenario where the three moving singular features interact, inducing a number of bifurcations. In such a scenario, the relation between the extracted ridges of the $|\nabla\Phi|$ field and the moving paths of those singular features is less clear and subject to the selection of the integration time T. More in-depth investigation is needed in order to discover a formal relation between the moving trajectory of a singular feature with certain ridge in the $|\nabla\Phi|$ field. This formal study will help determine the application of the rotation analysis based on streaklines to feature tracking.

VIII. Conclusion

In this work, we generalize the *winding angle* computation and present a unified 2D feature-based flow analysis and visualization framework. A Φ field and its gradient are computed by assigning the accumulated curvature value of the feature curve seeded from any given spatial location. This extends the utility beyond vortex identification to flow domain segmentation and unsteady flow. Our theoretical and experimental results show that the Φ field and its gradient $|\nabla\Phi|$, can not only reveal the flow rotation behaviors with different orientation (clockwise versus counter clockwise) but also highlight the structures that separate the sub-regions with these different flow rotations. In addition, we compare the flow structure obtained from the $|\nabla\Phi|$ field with the flow separation structure computed using the popular FTLE approach.

In general, we discover that our results contain not only the information of flow separation but also the information related to vortices and cycloid motion. Furthermore, we show the extension of our pipeline to streaklines where the FTLE method cannot be applied. In particular, we demonstrate the possible relation between the singular features (with zero vector values at certain time range) and the structure of $|\nabla\Phi|$ computed based on streaklines, indicating its potential application to feature tracking. The streakline-based Φ potentially offers an advantage relative to a pathline-based approach for unsteady vector fields because the pathline-based approach loses information about the temporal variation of the flow at its seed point while the streakline-based approach does not. This difference is manifested in our results because the streakline-based Φ is able to track the singularities in the flow while the pathline-based approach cannot.

Overall, we believe that the introduction of Φ field and its associated computation and analysis framework *may* help unify the previous flow analysis techniques that focus on either the translation property of the flow, e.g., topology and separation structure computation, or the flow kinematics, e.g., Jacobian analysis, although determining their formal relation requires more in-depth investigation.

In the future, it will be interesting to investigate the relation of Φ to the asymmetric tensor field decomposition [37] and the Helmholtz-Hodge decomposition [42]. It may also be interesting to explore the relation of the ridges of $|\nabla\Phi|$ based on streaklines and the recently introduced streakline based topology [25], [26]. There are also other technical and practical issues that this initial framework needs to address, such as the effects of numerical inaccuracy and sampling strategy, the cancellation of signed rotation, in addition to the improvement of the performance. Furthermore, how to extend this framework to 3D flow analysis will be an important topic for future research. This is because rotation can be ambiguous in 3D. A similar metric introduced in [32] can be employed for 3D flow. An additional consideration is that integral based on the velocity field is not Galilean invariant. To appropriately capture the rotational behavior of a translating vortex, it is necessary to observe particle motion in an appropriate reference frame moving with the vortex [43]. We plan to investigate this aspect in our future work. Finally, our current framework cannot be applied to *time lines*. This is because the initial seed for a time line is a 1D curve rather than 0D, i.e., a point. This additional degree of freedom will make the definition of a similar Φ field non-unique, i.e., different initial seed curves will lead to different Φ values under the same time frame. In the future, it will be interesting to adapt our current pipeline to incorporate time lines.

References

[1] G. Chen, K. Mischaikow, R. S. Laramee, P. Pilarczyk, and E. Zhang, "Vector field editing and periodic orbit extraction using Morse decomposition," *IEEE Transactions on Visualization and Computer Graphics*, vol. 13, no. 4, pp. 769–785, Jul./Aug. 2007.

[2] J. L. Helman and L. Hesselink, "Representation and display of vector field topology in fluid flow data sets," *IEEE Computer*, vol. 22, no. 8, pp. 27–36, August 1989.

[3] R. Laramee, H. Hauser, L. Zhao, and F. H. Post, "Topology based flow visualization: the state of the art," in *Topology-Based Methods in Visualization (Proceedings of Topo-in-Vis 2005)*, ser. Mathematics and Visualization. Springer, 2007, pp. 1–19.

[4] X. Tricoche, G. Scheuermann, and H. Hagen, "Continuous topology simplification of planar vector fields," in *Proceedings of IEEE Visualization 2001*, 2001, pp. 159–166.

[5] G. Haller, "Lagrangian coherent structures and the rate of strain in two-dimensional turbulence," *Phys. Fluids A*, vol. 13, pp. 3365–3385, 2001.

[6] B. R. Munson, D. F. Young, and T. H. Okiishi, *Fundamentals of fluid mechanics*. New York, 1990.

[7] I. Sadarjoen and F. Post, "Geometric methods for vortex extraction," in *Proc. EG/IEEE Visualization Symposium*, 1999.

[8] M. Edmunds, R. S. Laramee, G. Chen, N. Max, E. Zhang, and C. Ware, "Surface-based flow visualization," *Computers & Graphics*, vol. 36, no. 8, pp. 974–990, 2012.

[9] M. Jiang, R. Machiraju, and D. Thompson, "Detection and visualization of vortices," in *The Visualization Handbook*. Academic Press, 2005, pp. 295–309.

[10] A. Pobitzer, R. Peikert, R. Fuchs, B. Schindler, A. Kuhn, H. Theisel, K. Matkovic, and H. Hauser, "The state of the art in topology-based visualization of unsteady flow," *Computer Graphics Forum*, vol. 30, no. 6, pp. 1789–1811, September 2011. [Online]. Available: http://dx.doi.org/10.1111/j.1467-8659.2011.01901.x

[11] T. Salzbrunn, T. Wischgoll, H. Jänicke, and G. Scheuermann, "The state of the art in flow visualization: Partition-based techniques," in *In Simulation and Visualization 2008 Proceedings*, H. Hauser, S. Strassburger, and H. Theisel, Eds. SCS Publishing House, 2008, pp. 75–92.

[12] K. Polthier and E. Preuß, "Identifying vector fields singularities using a discrete hodge decomposition," in *Mathematical Visualization III*. Ed: H.C. Hege, K. Polthier, 2003, pp. 112–134.

[13] G. Scheuermann, H. Hagen, H. Krüger, M. Menzel, and A. Rockwood, "Visualization of higher order singularities in vector fields," in *Proceedings of IEEE Visualization '97*, Oct. 1997, pp. 67–74. [Online]. Available: http://visinfo.zib.de/EVlib/Show?EVL-1997-121

[14] H. Theisel, T. Weinkauf, and H.-P. Seidel, "Grid-independent detection of closed stream lines in 2D vector fields," in *Proceedings of the Conference on Vision, Modeling and Visualization 2004 (VMV 04)*, Nov. 2004, pp. 421–428.

[15] T. Wischgoll and G. Scheuermann, "Detection and visualization of closed streamlines in planar fields," *IEEE Transactions on Visualization and Computer Graphics*, vol. 7, no. 2, pp. 165–172, 2001.

[16] G. Chen, K. Mischaikow, R. S. Laramee, and E. Zhang, "Efficient Morse decompositions of vector fields," *IEEE Transactions on Visualization and Computer Graphics*, vol. 14, no. 4, pp. 848–862, Jul./Aug. 2008.

[17] J. Reininghaus, C. Lowen, and I. Hotz, "Fast combinatorial vector field topology," *IEEE Transactions on Visualization and Computer Graphics*, vol. 17, no. 10, pp. 1433–1443.

[18] R. Forman, "Combinatorial vector fields and dynamical systems," *Mathematische Zeitschrift*, vol. 228, pp. 629–681, 1998.

[19] W. Reich and G. Scheuermann, "Analysis of streamline separation at infinity using time-discrete markov chains," *IEEE Transactions on Visualization and Computer Graphics*, vol. 18, no. 12, pp. 2140–2148, 2012.

[20] F. Lekien, S. Shadden, and J. Marsden, "Lagrangian coherent structures in n-dimensional systems," *Journal of Mathematical Physics*, vol. 48, no. 6, p. Art. No. 065404, 2007.

[21] S. Shadden, F. Lekien, and J. Marsden, "Definition and properties of lagrangian coherent structures from finite-time lyapunov exponents in two-dimensional aperiodic flows," *Physica D*, vol. 212, no. 3–4, pp. 271–304, 2005.

[22] F. Sadlo and R. Peikert, "Efficient visualization of lagrangian coherent structures by filtered amr ridge extraction," *IEEE Transactions on Visualization and Computer Graphics*, vol. 13, no. 6, pp. 1456–1463, 2007.

[23] ——, "Visualizing lagrangian coherent structures and comparison to vector field topology," in *Topology-Based Methods in Visualization II*. Springer, 2008, pp. 15–30.

[24] C. Garth, A. Wiebel, X. Tricoche, K. I. Joy, and G. Scheuermann, "Lagrangian visualization of flow-embedded surface structures," *Computer Graphics Forum*, vol. 27, no. 3, pp. 1007–1014, 2008.

[25] F. Sadlo and D. Weiskopf, "Time-dependent 2-d vector field topology: An approach inspired by lagrangian coherent structures," *Comput. Graph. Forum*, vol. 29, no. 1, pp. 88–100, 2010.

[26] M. Üffinger, F. Sadlo, and T. Ertl, "A time-dependent vector field topology based on streak surfaces," *IEEE Trans. Vis. Comput. Graph.*, vol. 19, no. 3, pp. 379–392, 2013.

[27] T. Salzbrunn and G. Scheuermann, "Streamline predicates," *IEEE Transactions on Visualization and Computer Graphics*, vol. 12, no. 6, pp. 1601–1612, 2006.

[28] T. Salzbrunn, C. Garth, G. Scheuermann, and J. Meyer, "Pathline predicates and unsteady flow structures," *The Visual Computer*, vol. 24, no. 12, pp. 1039–1051, 2008.

[29] K. Shi, H. Theisel, H. Hauser, T. Weinkauf, K. Matkovic, H.-C. Hege, and H.-P. Seidel, "Path line attributes - an information visualization approach to analyzing the dynamic behavior of 3D time-dependent flow fields," in *Topology-Based Methods in Visualization II*, ser. Mathematics and Visualization, H.-C. Hege, K. Polthier, and G. Scheuermann, Eds. Grimma, Germany: Springer, 2009, pp. 75–88.

[30] A. Pobitzer, A. Lez, K. Matkovic, and H. Hauser, "A statistics-based dimension reduction of the space of path line attributes for interactive visual flow analysis," in *PacificVis*, 2012, pp. 113–120.

[31] H. Yu, C. Wang, C.-K. Shene, and J. H. Chen, "Hierarchical streamline bundles," *IEEE Transactions on Visualization and Computer Graphics*, vol. 18, no. 8, pp. 1353–1367, Aug. 2012. [Online]. Available: http://dx.doi.org/10.1109/TVCG.2011.155

[32] T. McLoughlin, M. W. Jones, R. S. Laramee, R. Malki, I. Masters, and C. D. Hansen, "Similarity measures for enhancing interactive streamline seeding," *IEEE Transactions on Visualization and Computer Graphics*, vol. 19, no. 8, pp. 1342–1353, 2013.

[33] C. Wang and H.-W. Shen, "Information theory in scientific visualization," *Entropy*, vol. 13, no. 1, pp. 254–273, 2011. [Online]. Available: http://www.mdpi.com/1099-4300/13/1/254

[34] L. Xu, T.-Y. Lee, and H.-W. Shen, "An information-theoretic framework for flow visualization," *IEEE Transactions on Visualization and Computer Graphics*, vol. 16, no. 6, pp. 1216–1224, 2010.

[35] K. Lu, A. Chaudhuri, T.-Y. Lee, H. W. Shen, and P. C. Wong, "Exploring vector fields with distribution-based streamline analysis," in *Proceeding of PacificVis '13: IEEE Pacific Visualization Symposium*, Sydney, Australia, march 2013.

[36] G. Chen, D. Palke, Z. Lin, H. Yeh, P. Vincent, R. S. Laramee, and E. Zhang, "Asymmetric tensor field visualization for surfaces," *IEEE Transactions on Visualization and Computer Graphics*, vol. 17, no. 12, pp. 1979–1988, Nov. 2011. [Online]. Available: http://dx.doi.org/10.1109/TVCG.2008.68

[37] E. Zhang, H. Yeh, Z. Lin, and R. S. Laramee, "Asymmetric tensor analysis for flow visualization," *IEEE Transactions on Visualization and Computer Graphics*, vol. 15, no. 1, pp. 106–122, 2009.

[38] R. S. Laramee, D. Weiskopf, J. Schneider, and H. Hauser, "Investigating swirl and tumble flow with a comparison of visualization techniques," in *Proceedings of IEEE Visualization '04*, 2004, pp. 51–58.

[39] R. Peikert and M. Roth, "The "parallel vectors" operator: a vector field visualization primitive," in *VIS '99: Proceedings of the conference on Visualization '99*. Los Alamitos, CA, USA: IEEE Computer Society Press, 1999, pp. 263–270.

[40] T. Weinkauf and H. Theisel, "Streak lines as tangent curves of a derived vector field," *IEEE Transactions on Visualization and Computer Graphics (Proceedings Visualization 2010)*, vol. 16, no. 6, pp. 1225–1234, November - December 2010.

[41] J. Kasten, J. Reininghaus, I. Hotz, and H.-C. Hege, "Two-dimensional time-dependent vortex regions based on the acceleration magnitude," *Transactions on Visualization and Computer Graphics (Vis'11)*, vol. 17, no. 12, pp. 2080–2087, 2011.

[42] H. Bhatia, G. Norgard, V. Pascucci, and P.-T. Bremer, "The helmholtz-hodge decomposition - a survey," *IEEE Transactions on Visualization and Computer Graphics*, vol. 19, no. 8, pp. 1386–1404, 2013.

[43] T. Weinkauf, J. Sahner, H. Theisel, and H.-C. Hege, "Cores of swirling particle motion in unsteady flows," *IEEE Transactions on Visualization and Computer Graphics (Proceedings Visualization 2007)*, vol. 13, no. 6, pp. 1759–1766, November – December 2007. [Online]. Available: http://tinoweinkauf.net/publications/absweinkauf07c.html